Annals of Nuclear Energy 84 (2015) 19–30

Contents lists available at ScienceDirect

Annals of Nuclear Energy

journal homepage: www.elsevier.com/locate/anucene

Development of three-dimensional capabilities for modelling stationary fluctuations in nuclear reactor cores

Christophe Demazière *, Victor Dykin, Augusto Hernández-Solís [1], Viktor Boman [2]

Chalmers University of Technology, Department of Applied Physics, Division of Nuclear Engineering, SE-412 96 Gothenburg, Sweden

ARTICLE INFO

Article history:
Received 31 March 2014
Accepted 22 September 2014
Available online 3 November 2014

Keywords:
LWR multi-physics
Noise analysis
Neutron transport
Fluid dynamics
Heat transfer

ABSTRACT

This paper presents the development of a numerical tool meant at modelling the effect of stationary fluctuations in nuclear cores for systems cooled with either liquid water or boiling water. The originating fluctuations are defined for the variables describing the boundary conditions of the system, i.e. inlet velocity, inlet enthalpy, and outlet pressure. The tool then determines in the frequency domain the three-dimensional distributions within the core of the corresponding fluctuations in neutron flux, coolant density, coolant velocity, coolant enthalpy, and fuel temperature. The tool is thus based on the simultaneous modelling of neutron transport, fluid dynamics, and heat transfer in a truly integrated and fully coupled manner. The modelling of neutron transport relies on the two-group diffusion approximation and a spatial discretization based on finite differences. The modelling of fluid dynamics is performed using the Homogeneous Equilibrium Model, with a void fraction correction based on a pre-computed distribution of the static slip ratio (when two-phase flow conditions are encountered). Heat conduction in the fuel pins is also accounted for, and the heat transfer between the fuel pins and the coolant is modelled also using a pre-computed distribution of the heat transfer coefficient. The spatial discretization of the fluid dynamic and heat transfer problems is carried out using finite volumes. The tool, currently entirely Matlab based, requires minimal input data, mostly in form of the three-dimensional distributions of the macroscopic cross-sections and their relative dependence on coolant density and fuel temperature, the point-kinetic parameters of the core, as well as the three-dimensional distribution of the slip ratio (in case of two-phase flow conditions) and of the heat transfer coefficient. Such data can be provided by any static core simulator that thus needs to be run prior to using the present tool. In addition to briefly summarizing the different test cases used to verify the code, the paper also presents the results of simulations performed for a typical Pressurized Water Reactor and for a typical Boiling Water Reactor, as illustrations of the capabilities of the tool.

1. Introduction

The Division of Nuclear Engineering at Chalmers University of Technology, Gothenburg, Sweden has been very active for the past ten years in developing computational methods allowing the estimation of the so-called reactor transfer functions for actual reactor cores. The reactor transfer function gives the spatial and energy distribution of the neutron noise induced by any arbitrary noise source. Due to the multi-physics and multi-scale aspects of the systems at hand, the development of computational procedures for reactor transfer function estimation was carried out in several successive steps.

The first developments were not considering the interdependence between neutron transport and fluid dynamics/heat transfer in an explicit manner. Rather, a given physical perturbation in the system (perturbation in temperature, flow velocity, etc.) was directly expressed as a perturbation in the parameters appearing in the conservation equations expressing neutron transport, i.e. the macroscopic nuclear cross-sections. In addition, the possible resulting neutron noise was assumed not to affect the thermal–hydraulic variables (i.e. flow conditions and heat transfer). As such, such simulations are referred to as open-loop reactor transfer function simulations, since the feedback from neutron transport onto fluid transport and heat transfer is not considered. The development of such capabilities was based on two-group diffusion theory,

* Corresponding author.
[1] Current affiliation: Royal Institute of Technology, Department of Physics, Division of Nuclear Power Safety, SE-106 91 Stockholm, Sweden.
[2] Current affiliation: Alten Sweden AB, A Odhners gata 41, SE-42130 Västra Frölunda, Sweden.

http://dx.doi.org/10.1016/j.anucene.2014.09.042
0306-4549/

and resulted in a code called CORE SIM, which is freely available (Demazière, 2011a).

More recently, a thermal–hydraulic module was developed, so that the closed-loop reactor transfer function could also be estimated, i.e. the interdependence between the different physical phenomena is fully accounted for within the tool. The thermal–hydraulic module is based on solving the mass, momentum, and enthalpy conservation equations for the fluid, and on solving the heat conduction equation in the solid fuel pellets. Both one-phase flow situations (Larsson and Demazière, 2012) and two-phase flows situations (Dykin et al., 2014) can be handled. Because of the fully coupled neutronic/thermal–hydraulic character of the tool, the noise source can be directly defined in more realistic terms such as perturbations of the flow velocity, temperature, etc. at the inlet of the core.

The coupled tool, in addition to be the only one of its kind, has a wide range of applicability. Any light-water reactor loaded with rectangular-type fuel assemblies can be modelled by the coupled tool, which is able to estimate the three-dimensional distributions of the stationary fluctuations of any neutronic and thermal–hydraulic variables in the core. The current version of the tool is implemented in Matlab.

In this paper, an overview of the models and algorithms used in the coupled code is first given, with emphasis on the modelling of neutron transport, on the modelling of fluid dynamics and heat transfer, and on the coupling methodology. The different test cases used to verify the developed tool are also briefly touched upon. Thereafter, two examples are presented as illustrations of the capabilities of the tool: a Pressurized Water Reactor (PWR) example, and a Boiling Water Reactor (BWR) example.

2. Overview of the models and algorithms

The modelling of neutron transport, fluid dynamics and heat transfer, is essentially based on volume-averaging the corresponding local conservation equations on adequate volumes, and on choosing a spatial discretization scheme. In the following, the local governing equations and their volume-averaged version are recalled for neutron transport and fluid dynamics/heat transfer, respectively. Since the solution to the dynamical problem requires the prior determination of the steady-state solution using the same spatial discretization scheme, the solution procedure for both static and dynamic calculations is detailed. Finally, some explanations about the coupling procedure between neutron transport and fluid dynamics and heat transfer are given.

2.1. Neutron transport modelling

The modelling of neutron transport relies on diffusion theory, which corresponds to a low-order approximation of the angular dependence of the neutron flux. Regarding the energy-dependence, two-group theory is used. The time-dependent local conservation equations for the neutron densities can thus be written as:

$$\frac{1}{v_1}\frac{\partial}{\partial t}\phi_1(\mathbf{r},t) = \nabla\cdot\left[D_{1,0}(\mathbf{r})\nabla\phi_1(\mathbf{r},t)\right] + \left[(1-\beta)\upsilon\Sigma_{f,1}(\mathbf{r},t) - \Sigma_{a,1}(\mathbf{r},t) - \Sigma_r(\mathbf{r},t)\right]\phi_1(\mathbf{r},t) + (1-\beta)\upsilon\Sigma_{f,2}(\mathbf{r},t)\phi_2(\mathbf{r},t) + \lambda C(\mathbf{r},t) \tag{1}$$

$$\frac{1}{v_2}\frac{\partial}{\partial t}\phi_2(\mathbf{r},t) = \nabla\cdot\left[D_{2,0}(\mathbf{r})\nabla\phi_2(\mathbf{r},t)\right] + \Sigma_r(\mathbf{r},t)\phi_1(\mathbf{r},t) - \Sigma_{a,2}(\mathbf{r},t)\phi_2(\mathbf{r},t) \tag{2}$$

for the fast and thermal groups, respectively, whereas the local balance equation for the one-group precursors of delayed neutrons is given as:

$$\frac{\partial C(\mathbf{r},t)}{\partial t} = \beta\upsilon\Sigma_{f,1}(\mathbf{r},t)\phi_1(\mathbf{r},t) + \beta\upsilon\Sigma_{f,2}(\mathbf{r},t)\phi_2(\mathbf{r},t) - \lambda C(\mathbf{r},t) \tag{3}$$

The previous equations use standard notations, and the macroscopic removal cross-section is defined as:

$$\Sigma_r(\mathbf{r},t) = \Sigma_{s0,1\to 2}(\mathbf{r},t) - \frac{\Sigma_{s0,2\to 1}(\mathbf{r},t)\phi_2(\mathbf{r},t)}{\phi_1(\mathbf{r},t)} \tag{4}$$

It has to be mentioned that all macroscopic cross-sections are allowed to vary with time, except the diffusion coefficients. This later assumption was demonstrated to have a negligible impact on the solution (Larsson and Demazière, 2009). The above equations are also based on the assumption that the energy cut-off between the fast and thermal energy groups is below the energy at which the prompt and delayed neutron emissions occur.

Integrating the previous balance equations on a node n having a volume V_n in a Cartesian coordinate system leads to:

$$\frac{1}{v_1}\frac{\partial}{\partial t}\phi_{1,n}(t) = -\sum_{\aleph=x,y,z}\left[a^{\aleph}_{1,n}\phi_{1,n}(t) + b^{\aleph}_{1,n}\phi_{1,n+1}(t) + c^{\aleph}_{1,n}\phi_{1,n-1}(t)\right] + \left[(1-\beta)\upsilon\Sigma_{f,1,n}(t) - \Sigma_{a,1,n}(t) - \Sigma_{r,n}(t)\right]\phi_{1,n}(t) + (1-\beta)\upsilon\Sigma_{f,2,n}(t)\phi_{2,n}(t) + \lambda C_n(t) \tag{5}$$

$$\frac{1}{v_2}\frac{\partial}{\partial t}\phi_{2,n}(t) = -\sum_{\aleph=x,y,z}\left[a^{\aleph}_{2,n}\phi_{2,n}(t) + b^{\aleph}_{2,n}\phi_{2,n+1}(t) + c^{\aleph}_{2,n}\phi_{2,n-1}(t)\right] + \Sigma_{r,n}(t)\phi_{1,n}(t) - \Sigma_{a,2,n}(t)\phi_{2,n}(t) \tag{6}$$

$$\frac{\partial C_n(t)}{\partial t} = \beta\upsilon\Sigma_{f,1,n}(t)\phi_{1,n}(t) + \beta\upsilon\Sigma_{f,2,n}(t)\phi_{2,n}(t) - \lambda C_n(t) \tag{7}$$

The nodes are chosen as being axial slices of entire fuel assemblies or of sections of fuel assemblies. In order to guarantee consistency with the thermal–hydraulic models, the nodes should always contain the fluid and the fuel. The above discretized equations were obtained using finite differences, and consequently the between nodes-coupling coefficients $a^{\aleph}_{g,n}$, $b^{\aleph}_{g,n}$, and $c^{\aleph}_{g,n}$, which only depends on the time-independent diffusion coefficients, are in turn time-independent. The reason for using finite differences lies with the fact that no numerical or convergence problem is to be expected with such a scheme. Having a robust scheme was of prime importance when developing the tool reported hereafter. The volume-averaged quantities are estimated according to:

$$\phi_{g,n}(t) = \frac{1}{V_n}\int_{V_n}\phi_g(\mathbf{r},t)d^3\mathbf{r} \tag{8}$$

and

$$\Sigma_{g,n}(t) = \frac{\int_{V_n}\Sigma_g(\mathbf{r},t)\phi_g(\mathbf{r},t)d^3\mathbf{r}}{V_n\phi_{g,n}(t)} \tag{9}$$

so that the actual reaction rates are preserved.

Although the tool is meant at calculating the effect of stationary fluctuations, the solution to the static case is first required. As will be demonstrated in Eqs. (14) and (15), the effect of driving fluctuations of any macroscopic cross-section onto the neutron balance equations is normalized by the static neutron fluxes. In steady-state conditions, Eqs. (5)–(7) become:

$$-\sum_{\aleph=x,y,z}\left(a^{\aleph}_{1,n}\phi_{1,n,0} + b^{\aleph}_{1,n}\phi_{1,n+1,0} + c^{\aleph}_{1,n}\phi_{1,n-1,0}\right) + \left(\frac{\upsilon\Sigma_{f,1,n,0}}{k_{eff}} - \Sigma_{a,1,n,0} - \Sigma_{r,n,0}\right)\phi_{1,n,0} + \frac{\upsilon\Sigma_{f,2,n,0}}{k_{eff}}\phi_{2,n,0} = 0 \tag{10}$$

$$-\sum_{\aleph=x,y,z}\left(a^{\aleph}_{2,n}\phi_{2,n,0}+b^{\aleph}_{2,n}\phi_{2,n+1,0}+c^{\aleph}_{2,n}\phi_{2,n-1,0}\right)+\Sigma_{r,n,0}\phi_{1,n,0}-\Sigma_{a,2,n,0}\phi_{2,n,0}=0 \quad (11)$$

where the subscript 0 denotes the steady-state value of the macroscopic cross-sections and neutron fluxes. In the equations above, the fission sources are normalized by the effective multiplication factor of the system, in order to guarantee time-independent neutron balance equations in case the system is not perfectly critical. Constructing a vector column $\mathbf{\Phi}$ containing the nodal scalar neutron flux values in the fast and thermal groups, Eqs. (10) and (11) can be rewritten in a more compact form as:

$$\mathbf{M}^{sta}\times\mathbf{\Phi}=\frac{1}{k_{eff}}\mathbf{F}^{sta}\times\mathbf{\Phi} \quad (12)$$

where $\mathbf{M}^{sta}$ and $\mathbf{F}^{sta}$ are matrices. Eq. (12) is an eigenvalue equation, which is solved using an explicitly-restarted Arnoldi algorithm. In case of convergence problem, a power iteration method with Wielandt's shift technique is also available. Further details about the implementation of these two methods can be found in Demazière (2011a,b).

In case of stationary fluctuations, any time-dependent term, generically denoted as $X_n(t)$, can be split into a mean value $X_{n,0}$ and a fluctuating part $\delta X_n(t)$ as:

$$X_n(t)=X_{n,0}+\delta X_n(t) \quad (13)$$

Using this expression in Eqs. (5)–(7), subtracting the static Eqs. (10) and (11), performing a temporal Fourier-transform, and neglecting second-order terms, the following balance equations are obtained:

$$\begin{aligned}\frac{i\omega}{v_1}\delta\phi_{1,n}(\omega)=&-\sum_{\aleph=x,y,z}\left[a^{\aleph}_{1,n}\delta\phi_{1,n}(\omega)+b^{\aleph}_{1,n}\delta\phi_{1,n+1}(\omega)+c^{\aleph}_{1,n}\delta\phi_{1,n-1}(\omega)\right]\\&+\left[\frac{v\Sigma_{f,1,n,0}}{k_{\text{eff}}}\left(1-\frac{i\omega\beta}{i\omega+\lambda}\right)-\Sigma_{a,1,n,0}-\Sigma_{r,n,0}\right]\delta\phi_{1,n}(\omega)\\&+\frac{v\Sigma_{f,2,n,0}}{k_{\text{eff}}}\left(1-\frac{i\omega\beta}{i\omega+\lambda}\right)\delta\phi_{2,n}(\omega)\\&+\left[\frac{\delta v\Sigma_{f,1,n}(\omega)}{k_{\text{eff}}}\left(1-\frac{i\omega\beta}{i\omega+\lambda}\right)-\delta\Sigma_{a,1,n}(\omega)-\delta\Sigma_{r,n}(\omega)\right]\phi_{1,n,0}\\&+\frac{\delta v\Sigma_{f,2,n}(\omega)}{k_{\text{eff}}}\left(1-\frac{i\omega\beta}{i\omega+\lambda}\right)\phi_{2,n,0}\end{aligned} \quad (14)$$

$$\begin{aligned}\frac{i\omega}{v_2}\delta\phi_{2,n}(\omega)=&-\sum_{\aleph=x,y,z}\left[a^{\aleph}_{2,n}\delta\phi_{2,n}(\omega)+b^{\aleph}_{2,n}\delta\phi_{2,n+1}(\omega)+c^{\aleph}_{2,n}\delta\phi_{2,n-1}(\omega)\right]\\&+\Sigma_{r,n,0}\delta\phi_{1,n}(\omega)-\Sigma_{a,2,n,0}\delta\phi_{2,n}(\omega)\\&+\delta\Sigma_{r,n}(\omega)\phi_{1,n,0}-\delta\Sigma_{a,2,n}(\omega)\phi_{2,n,0}\end{aligned} \quad (15)$$

Constructing a vector column $\boldsymbol{\delta\Phi}$ containing the fluctuations of the nodal scalar neutron flux in the fast and thermal groups, Eqs. (14) and (15) can be rewritten in a more compact form as:

$$\mathbf{M}^{dyn}\times\boldsymbol{\delta\Phi}=\mathbf{S} \quad (16)$$

where $\mathbf{M}^{dyn}$ is a matrix and $\mathbf{S}$ is a column vector containing the fluctuations of the macroscopic cross-sections. Eq. (16) is a non-homogeneous problem, which is solved by first factorizing the matrix $\mathbf{M}^{dyn}$ into a unit sparse lower triangular matrix and an upper sparse triangular matrix using the UMFPACK package (Davis, 2002), and by then performing forward/backward substitutions. Further details about the implementation of the solution procedure can be found in Demazière (2011a,b).

The neutronic static and dynamic solvers were successfully verified and benchmarked for a number of test cases summarized below:

- A one-region one-dimensional critical system.
- A two-region one-dimensional critical system.
- A one-region two-dimensional critical system.
- Heterogeneous three-dimensional critical systems (for static calculations only).

The piece-wise homogeneous test cases were compared against analytical and semi-analytical solutions, whereas the static heterogeneous test cases were compared against the results of commercial static core simulators. The description of these test cases and the comparisons between the numerical solutions and the reference solutions are detailed in Demazière (2011c).

2.2. Thermal–hydraulic modelling

The thermal–hydraulic modelling relies on the time-dependent balance equations expressing locally the conservation of mass, linear momentum, and enthalpy in the coolant region and on the time-dependent temperature local conservation equation in the fuel region. Those balance equation in the fluid read as:

$$\frac{\partial}{\partial t}\rho(\mathbf{r},t)+\nabla\cdot[\rho(\mathbf{r},t)\mathbf{v}(\mathbf{r},t)]=0 \quad (17)$$

$$\begin{aligned}&\frac{\partial}{\partial t}[\rho(\mathbf{r},t)\mathbf{v}(\mathbf{r},t)]+\nabla\cdot[\rho(\mathbf{r},t)\mathbf{v}(\mathbf{r},t)\otimes\mathbf{v}(\mathbf{r},t)]\\&\quad=\nabla\cdot\tau(\mathbf{r},t)-\nabla P(\mathbf{r},t)+\mathbf{g}\rho(\mathbf{r},t)\end{aligned} \quad (18)$$

$$\frac{\partial}{\partial t}[\rho(\mathbf{r},t)h(\mathbf{r},t)]+\nabla\cdot[\rho(\mathbf{r},t)\mathbf{v}(\mathbf{r},t)h(r,t)]\approx-\nabla\cdot\mathbf{q}''(\mathbf{r},t) \quad (19)$$

whereas in the solid fuel region, the heat conduction equation reads as:

$$\rho(T)c(T)\frac{\partial}{\partial t}T(\mathbf{r},t)=\nabla\cdot[k\nabla T(\mathbf{r},t)]+q'''(\mathbf{r},t) \quad (20)$$

The previous equations use standard notations. In Eq. (19), only the source term related to the addition of heat by the fuel assemblies is retained on the right-hand side of the equation, which is thus approximate. Nevertheless, due to the much larger amplitude of this contribution compared with the other source terms (work corresponding to the effect of the stresses, of the pressure, and of the gravity force), such an approximation is valid for reactor applications.

Integrating the previous balance Eqs. (17)–(19) for the fluid, assumed to be mono-directional along the vertical z-axis, on a node m having a volume V_m (being a sub-volume of V_n earlier defined and being entirely occupied by the fluid) and cross-section area $A^{\pm}_n$ (the superscript + representing the outward cross-sectional flow area to the node, and the superscript – representing the inward cross-section flow area to the node) leads to:

$$V_m\frac{\partial}{\partial t}\rho_m(t)+\left[A^+_m\rho^+_m(t)\hat{v}^+_{z,m}(t)-A^-_m\rho^-_m(t)\hat{v}^-_{z,m}(t)\right]=0 \quad (21)$$

$$\begin{aligned}&V_m\frac{\partial}{\partial t}[\rho_m(t)\hat{v}_{z,m}(t)]+\left\{A^+_m\rho^+_m(t)\left[\hat{v}^+_{z,m}(t)\right]^2-A^-_m\rho^-_m(t)\left[\hat{v}^-_{z,m}(t)\right]^2\right\}\\&\quad\approx-\frac{f_mV_m}{2D_e}\rho^-_{l,m}(t)\left[\hat{v}^-_{l,z,m}(t)\right]^2-\left[A^+_mP^+_m(t)-A^-_mP^-_m(t)\right]-gV_m\rho_m(t)\end{aligned} \quad (22)$$

$$\begin{aligned}&V_m\frac{\partial}{\partial t}\left[\rho_m(t)\hat{h}_m(t)\right]+\left[A^+_m\rho^+_m(t)\hat{v}^+_{z,m}(t)\hat{h}^+_m(t)-A^-_m\rho^-_m(t)\hat{v}^-_{z,m}(t)\hat{h}^-_m(t)\right]\\&\quad\approx-S_{m,surf}q''_{m,surf}(t)\end{aligned} \quad (23)$$

In the fluid dynamics model presented above, the inter-assembly and intra-assembly bypass flows are not taken into account.

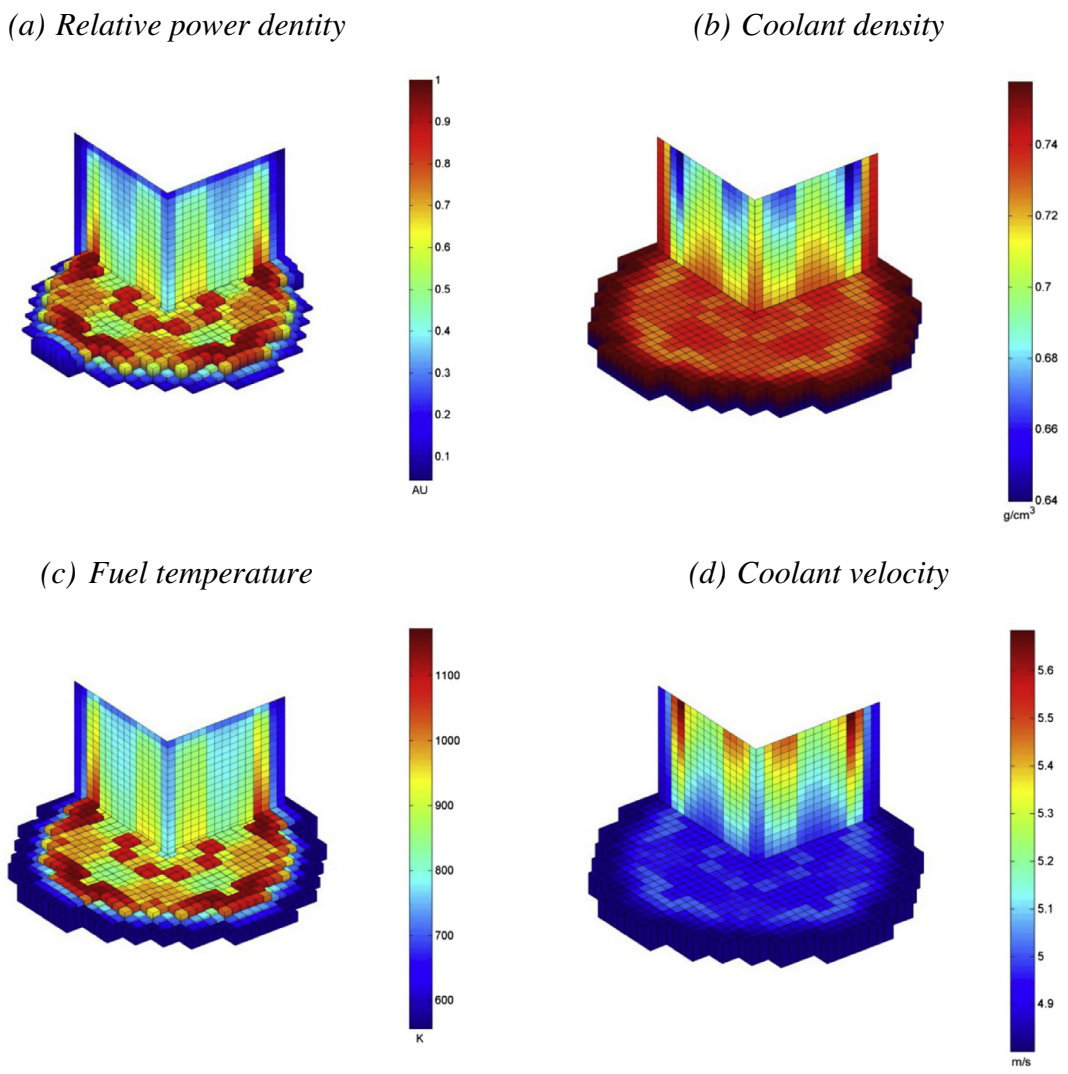

Fig. 1. Three-dimensional distributions of the static neutronic and thermal–hydraulic variables (PWR example). The horizontal planes give the radial distributions at ¼ elevation from the core bottom, whereas the vertical planes give the axial distributions through the middle of the core.

Integrating the heat conduction Eq. (20) on a node f having a volume V_f (being a sub-volume of V_n earlier defined and being entirely occupied by the fuel) leads to:

$$V_f \rho_f(T_f) c_f(T_f) \frac{\partial}{\partial t} T_f(t) = -S_{f,surf} q''_{f,surf}(t) + V_f q'''_f(t) \tag{24}$$

In the previous equations, the following notations and definitions are used for any time- and space-dependent parameter expressed in a generic fashion as $x(\mathbf{r}, t)$:

$$x_m(t) = \frac{1}{V_m} \int_{V_m} x(\mathbf{r}, t) d^3\mathbf{r} \tag{25}$$

$$\hat{x}_m(t) = \frac{1}{\rho_m(t) V_m} \int_{V_m} \rho(\mathbf{r}, t) x(\mathbf{r}, t) d^3\mathbf{r} \tag{26}$$

$$x^{\pm}_m(t) = \frac{1}{A^{\pm}_m} \int_{A^{\pm}_m} x(\mathbf{r}, t) d^2\mathbf{r} \tag{27}$$

$$\hat{x}^{\pm}_m(t) = \frac{1}{\rho^{\pm}_m(t) A^{\pm}_m} \int_{A^{\pm}_m} \rho(\mathbf{r}, t) x(\mathbf{r}, t) d^2\mathbf{r} \tag{28}$$

$$x_f(t) = \frac{1}{V_f} \int_{V_f} x(\mathbf{r}, t) d\mathbf{r} \tag{29}$$

$$q''_{m,surf}(t) = \frac{1}{S_{m,surf}} \int_{S_{m,surf}} \mathbf{q}''(r, t) \cdot \mathbf{n} d^2\mathbf{r} \tag{30}$$

$$q''_{f,surf}(t) = \frac{1}{S_{f,surf}} \int_{S_{f,surf}} \mathbf{q}''(r, t) \cdot \mathbf{n} d^2\mathbf{r} \tag{31}$$

with $S_{m,surf}$ being the cladding surface area in contact with the fluid in the node m, and with $S_{f,surf}$ being the corresponding fuel lateral surface area for the node f. Eq. (22) was obtained assuming that:

$$\int_{A^{\pm}_m} \rho(\mathbf{r}, t) v^2_z(\mathbf{r}, t) d^2\mathbf{r} \approx A^{\pm}_m \rho^{\pm}_m(t) \left[\hat{v}^{\pm}_{z,m}(t)\right]^2 \tag{32}$$

Eq. (22) is only considered when two-phase flow situations are encountered. Otherwise, the linear momentum conservation equation is not solved, and the pressure is thus assumed to be space- and time-independent. Eq. (23) was also obtained assuming that:

$$\int_{A^{\pm}_m} \rho(\mathbf{r}, t) v_z(\mathbf{r}, t) h(\mathbf{r}, t) d^2\mathbf{r} \approx A^{\pm}_m \rho^{\pm}_m(t) \hat{v}^{\pm}_{z,m}(t) \hat{h}^{\pm}_m(t) \tag{33}$$

It is further assumed that there is no accumulation/dissipation of heat in the cladding, and thus:

$$-S_{m,surf} q''_{m,surf}(t) = S_{f,surf} q''_{f,surf}(t) \tag{34}$$

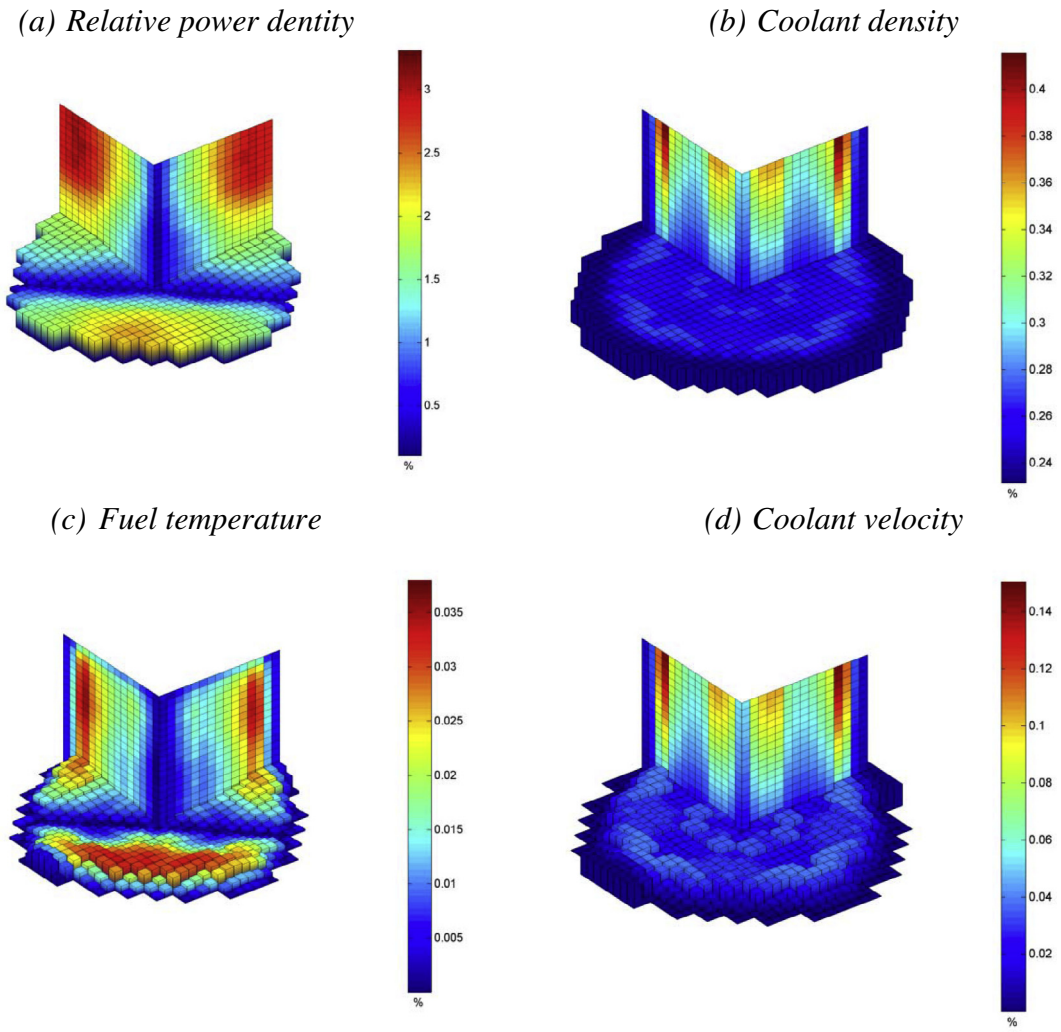

Fig. 2. Three-dimensional distributions of the amplitude of the stationary fluctuations of the neutronic and thermal–hydraulic variables (PWR example). The horizontal planes give the radial distributions at ¼ elevation from the core bottom, whereas the vertical planes give the axial distributions through the middle of the core.

In Eq. (22), f_m is the friction factor, D_e is the equivalent hydraulic diameter, and the subscript l in the corresponding friction pressure drop refers to the liquid phase only. The single-phase friction factor is based on McAdams' correlation (Rust, 1979), whereas the two-phase friction factor makes use of a two-phase friction multiplier based on Chisholm's correlation (Chisholm, 1973; Shah and Sekulic, 2003). Although many other correlations exist and could have been implemented and offered to the user of the tool, the present version of the tool is only based on Chisholm's correlation, thus simplifying the user's input preparation. Finally, in order to make use of the data provided by commercial static core simulators (such data are input data and necessary to run the models presented in this paper – see Section 3.1), the heat transferred between the fuel and the fluid for the node m is approximated using an effective heat transfer coefficient $h_{m,eff}$ as:

$$q''_{f,surf}(t) = h_{m,eff}\left[T_f(t) - T_m(t)\right] \tag{35}$$

In steady-state conditions, Eqs. (24) and (35) lead to the following evaluation of such an effective heat transfer coefficient:

$$h_{m,eff} = \frac{V_f q'''_{f,0}}{S_{f,surf}\left(T_{f,0} - T_{m,0}\right)} \tag{36}$$

where the subscript 0 represents steady-state values. In order to close the system of equations, some further approximations are necessary. The first approximation is to assume relationships between node-averaged values and area-averaged values of the form:

$$x_m(t) \approx \frac{x^+_m(t) + x^-_m(t)}{2} \tag{37}$$

and

$$\hat{x}_m(t) \approx \frac{\hat{x}^+_m(t) + \hat{x}^-_m(t)}{2} \tag{38}$$

In addition, a relationship between the state variables (for instance density, pressure, and enthalpy) is required. Such a relationship is given by the equation of state for the considered fluid. In case of two-phase flow situations, and assuming thermal and pressure equilibrium between the two phases, relationships between the phasic quantities and the mixture quantities are required. Those read as:

$$\rho_m(t) = \alpha_m(t)\rho_l(P_m) + [1 - \alpha_m(t)]\rho_v(P_m) \tag{39}$$

$$\rho^\pm_m(t) = \alpha^\pm_m(t)\rho_l(P^\pm_m) + \left[1 - \alpha^\pm_m(t)\right]\rho_v(P^\pm_m) \tag{40}$$

and

$$\hat{h}_m(t) = \frac{\alpha_m(t)\rho_l(P_m)h_l(P_m) + [1 - \alpha_m(t)]\rho_v(P_m)h_v(P_m)}{\rho_m(t)} \tag{41}$$

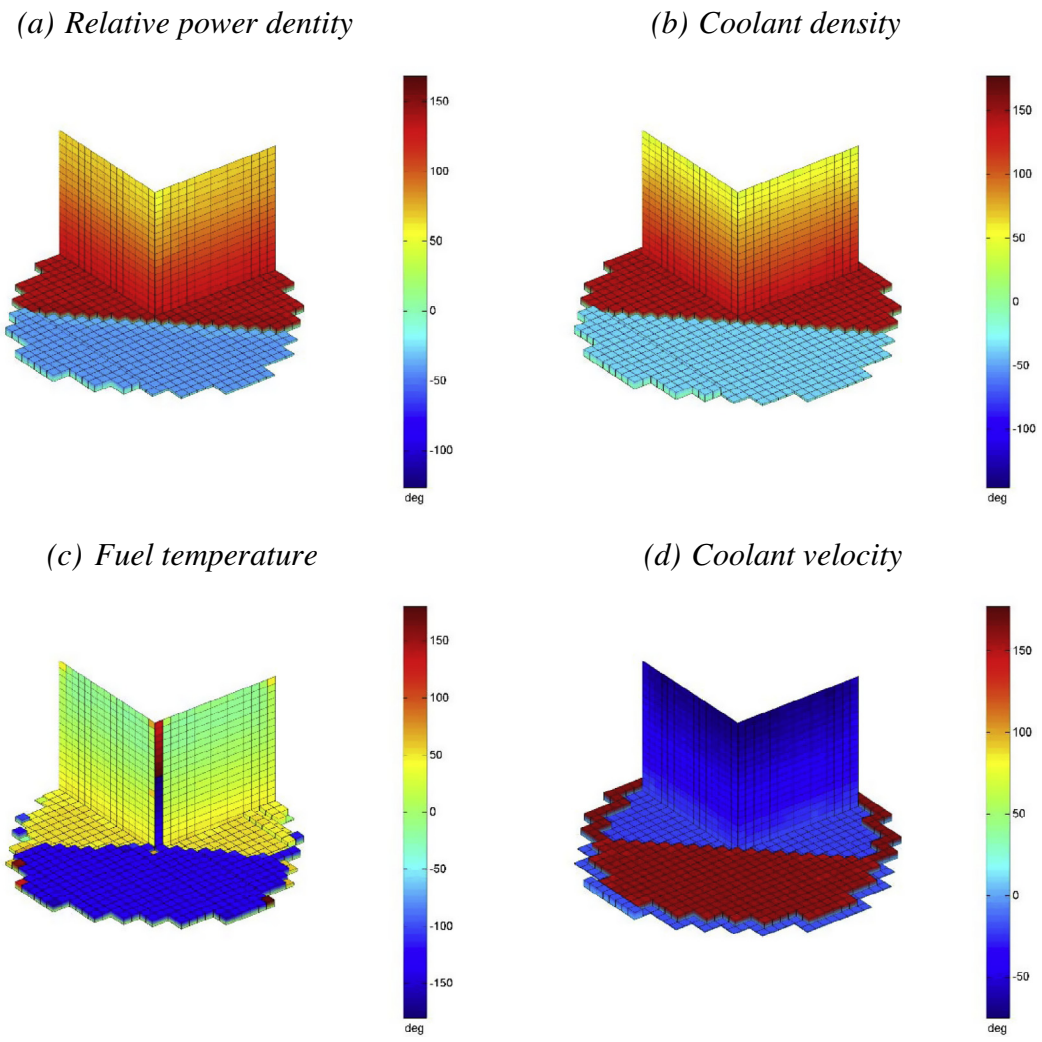

Fig. 3. Three-dimensional distributions of the phase of the stationary fluctuations of the neutronic and thermal–hydraulic variables (PWR example). The horizontal planes give the radial distributions at ¼ elevation from the core bottom, whereas the vertical planes give the axial distributions through the middle of the core.

$$\hat{h}_m^{\pm}(t) = \frac{\alpha_m^{\pm}(t)\rho_l(P_m^{\pm})h_l(P_m^{\pm}) + [1-\alpha_m^{\pm}(t)]\rho_v(P_m^{\pm})h_v(P_m^{\pm})}{\rho_m^{\pm}(t)} \tag{42}$$

where the subscripts l and v refer to the liquid phase and vapour phase, respectively. In the equations above, $\alpha_m(t)$ represents the volume-averaged void fraction, and $\alpha_m^{\pm}(t)$ represents the area-averaged void fraction. It has to be pointed out that the approximation introduced by Eq. (33) is equivalent to assume that the so-called dynamic mixture enthalpy (which is calculated using the mass flux as a weighting function) is identical to the mixture enthalpy as defined by Eqs. (41) and (42), for volume-averaged and area-averaged quantities, respectively. As a result, the drift velocity between the vapour and liquid phases is identically assumed to be equal to zero. The fluid model presented above thus corresponds to the classical Homogeneous Equilibrium Model (HEM). Such a model is known to over-predict the void fraction in the upper part of the fuel assemblies (Dokhane, 2004). In order to circumvent this problem and also considering the fact, as will be highlighted in Section 3a, that the results of static commercial core simulators are needed in order to use the present tool, the void fraction was adjusted as follows:

$$\alpha_m^{corr}(t) = \frac{1}{1-\frac{\hat{h}_m(t)-h_v(P_m)}{\hat{h}_m(t)-h_l(P_m)}\frac{\rho_v(P_m)}{\rho_l(P_m)}s_m} \tag{43}$$

$$\alpha_m^{\pm,corr}(t) = \frac{1}{1-\frac{\hat{h}_m^{\pm}(t)-h_v(P_m^{\pm})}{\hat{h}_m^{\pm}(t)-h_l(P_m^{\pm})}\frac{\rho_v(P_m^{\pm})}{\rho_l(P_m^{\pm})}s_m^{\pm}} \tag{44}$$

This adjustment was carried out using the volume-averaged slip ratio s_m and the area-averaged slip ratio $s_m^{\pm}$ provided by the static core simulator used to generate the data required to apply the numerical tool presented in this paper. Such distributions are thus estimated for all nodes throughout the entire core taken at steady-state conditions.

Although the tool is meant at calculating the effect of stationary fluctuations, the solution to the static case is first required. As will be demonstrated in Eqs. (52)–(55), the effect of driving fluctuations onto any thermal–hydraulic variable is normalized by the static thermal–hydraulic solution. In steady-state conditions and making use of Eq. (34), Eqs. (21)–(24) become:

$$A_m^+\rho_{m,0}^+\hat{v}_{z,m,0}^+ - A_m^-\rho_{m,0}^-\hat{v}_{z,m,0}^- = 0 \tag{45}$$

$$A_m^+\rho_{m,0}^+\left(\hat{v}_{z,m,0}^+\right)^2 - A_m^-\rho_{m,0}^-\left(\hat{v}_{z,m,0}^-\right)^2 \approx -\frac{f_m V_m}{2D_e}\rho_{l,m,0}^-\left(\hat{v}_{l,z,m,0}^-\right)^2 - \left(A_m^+P_{m,0}^+ - A_m^-P_{m,0}^-\right) - gV_m\rho_{m,0} \tag{46}$$

$$A_m^+\rho_{m,0}^+\hat{v}_{z,m,0}^+\hat{h}_{m,0}^+ - A_m^-\rho_{m,0}^-\hat{v}_{z,m,0}^-\hat{h}_{m,0}^- \approx S_{f,surf}q''_{f,surf,0} \tag{47}$$

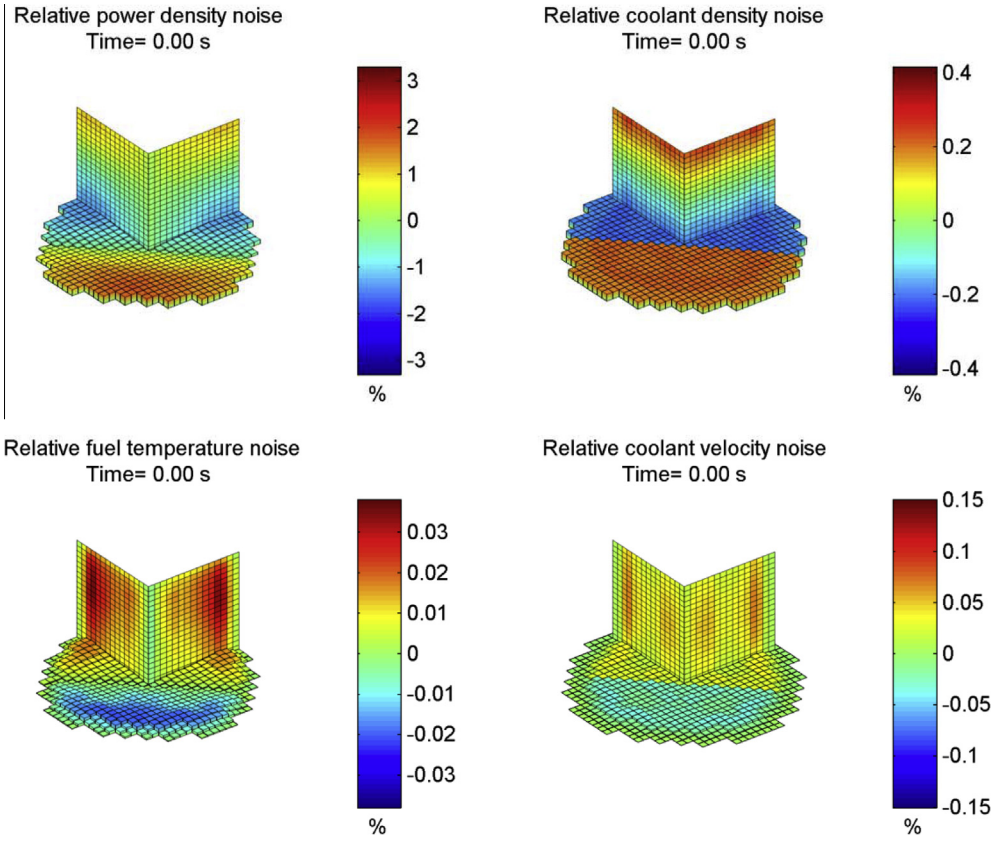

Fig. 4. Snapshot of the time-domain simulations showing the three-dimensional distributions of the stationary fluctuations of the neutronic and thermal–hydraulic variables (PWR example). The horizontal planes give the radial distributions at ¼ elevation from the core bottom, whereas the vertical planes give the axial distributions through the middle of the core.

$$0 = -S_{f,surf} q''_{f,surf,0} + V_f q'''_{f,0} \tag{48}$$

where the subscript 0 denotes steady-state values. In order to close the above system of equations, the equation of state of the fluid should be used, and the steady-state versions of Eqs. (37)–(39) and Eqs. (41)–(44) are also required (such steady-state equations are not presented here for the sake of clarity). In case of one-phase flow PWR conditions, the axial variation of the pressure field is negligible. As a result, the linear momentum conservation equation [Eq. (46)] is not solved, and the system of equations reduces to Eqs. 45, 47 and 48. Combining these equations results in:

$$A^+_m G^+_{m,0} - A^-_m G^-_{m,0} = 0 \tag{49}$$

$$A^+_m G^+_{m,0} \hat{h}^+_{m,0} - A^-_m G^-_{m,0} \hat{h}^-_{m,0} \approx -V_f q'''_{f,0} \tag{50}$$

with $G^{\pm}_{m,0} = \rho^{\pm}_{m,0} \hat{v}^{\pm}_{z,m,0}$ representing the mass flux. The above system of equations, together with the equation of state of the fluid, can be easily solved in each of the flow channels from the inlet of the core to the outlet, with given inlet boundary conditions. In case of two-phase flow BWR conditions, the pressure field needs to be resolved, and the system of equations given by Eqs. (45)–(48), together with the equation of state and the steady-state version of Eqs. (37)–(39) and Eqs. (41)–(44), are solved in an iterative manner as follows. The axial distributions of the pressure and enthalpy are first assumed, the axial variation of the velocity from the inlet to the outlet is then determined, followed by the re-calculation of the axial variation of the enthalpy and corresponding density from the inlet to the outlet. Based on the computed distributions, the pressure field is updated from the outlet to the inlet of the fuel channels, and the process is repeated until convergence. Further details about the calculation procedure can be found in Dykin et al. (2014).

In case of stationary fluctuations, any time-dependent term of the form $X_n(t)$ can be split into a mean value $X_{n,0}$ and a fluctuating part $\delta X_n(t)$ according to Eq. 13. Using these generic expressions in Eqs. (21)–(24), together with (35), subtracting the static Eqs. (45)–(48), performing a temporal Fourier-transform, and neglecting second-order terms, the following balance equations are obtained:

$$\begin{aligned} &i\omega V_m \delta\rho_m(\omega) + \left[A^+_m \delta\rho^+_m(\omega)\hat{v}^+_{z,m,0} - A^-_m \delta\rho^-_m(\omega)\hat{v}^-_{z,m,0}\right] \\ &\quad + \left[A^+_m \rho^+_{m,0}\delta\hat{v}^+_{z,m}(\omega) - A^-_m \rho^-_{m,0}\delta\hat{v}^-_{z,m}(\omega)\right] = 0 \end{aligned} \tag{51}$$

$$\begin{aligned} &i\omega V_m \delta\rho_m(\omega)\hat{v}_{z,m,0} + i\omega V_m \rho_{m,0}\delta\hat{v}_{z,m}(\omega) \\ &\quad + \left\{A^+_m \delta\rho^+_m(\omega)\left(\hat{v}^+_{z,m,0}\right)^2 - A^-_m \delta\rho^-_m(\omega)\left(\hat{v}^-_{z,m,0}\right)^2\right\} \\ &\quad + 2\left\{A^+_m \rho^+_{m,0}\hat{v}^+_{z,m,0}\delta\hat{v}^+_{z,m}(\omega) - A^-_m \rho^-_{m,0}\hat{v}^-_{z,m,0}\delta\hat{v}^-_{z,m}(\omega)\right\} \\ &\approx -\tfrac{f_m V_m}{2D_e}\delta\rho^-_{l,m}(\omega)\left(\hat{v}^-_{l,z,m,0}\right)^2 - \tfrac{f_m V_m}{D_e}\rho^-_{l,m,0}\delta\hat{v}^-_{l,z,m}(\omega) \\ &\quad - \left[A^+_m \delta P^+_m(\omega) - A^-_m \delta P^-_m(\omega)\right] - g V_m \delta\rho_m(\omega) \end{aligned} \tag{52}$$

$$\begin{aligned} &i\omega V_m \delta\rho_m(\omega)\hat{h}_{m,0} + i\omega V_m \rho_{m,0}\delta\hat{h}_m(\omega) \\ &\quad + \left[A^+_m \delta\rho^+_m(\omega)\hat{v}^+_{z,m,0}\hat{h}^+_{m,0} - A^-_m \delta\rho^-_m(\omega)\hat{v}^-_{z,m,0}\hat{h}^-_{m,0}\right] \\ &\quad + \left[A^+_m \rho^+_{m,0}\delta\hat{v}^+_{z,m}(\omega)\hat{h}^+_{m,0} - A^-_m \rho^-_{m,0}\delta\hat{v}^-_{z,m}(\omega)\hat{h}^-_{m,0}\right] \\ &\quad + \left[A^+_m \rho^+_{m,0}\hat{v}^+_{z,m,0}\delta\hat{h}^+_m(\omega) - A^-_m \rho^-_{m,0}\hat{v}^-_{z,m,0}\delta\hat{h}^-_m(\omega)\right] \\ &\approx -S_{m,surf} h_{m,eff}\left[\delta T_f(\omega) - \delta T_m(\omega)\right] \end{aligned} \tag{53}$$

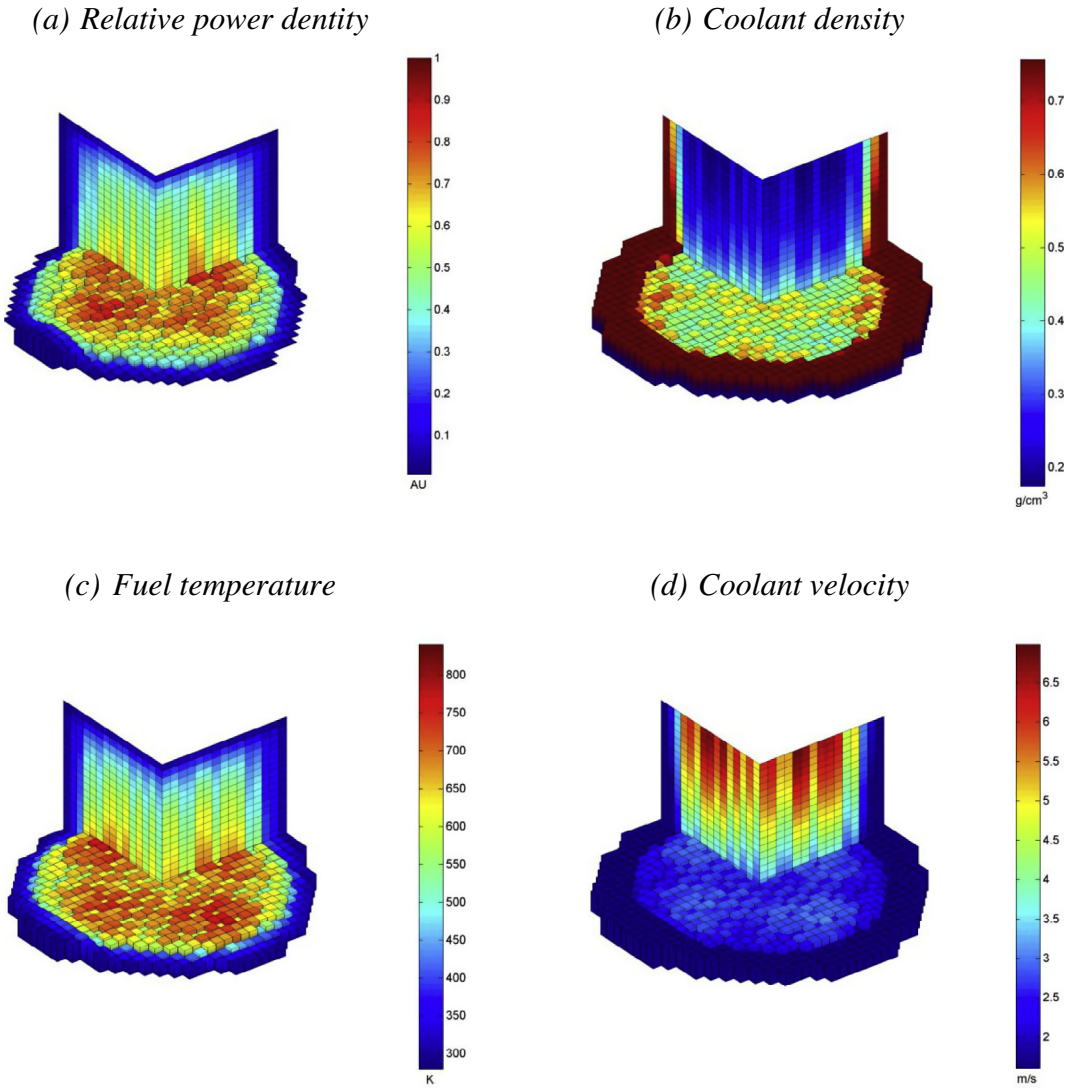

Fig. 5. Three-dimensional distributions of the static neutronic and thermal–hydraulic variables (BWR example). The horizontal planes give the radial distributions at ¼ elevation from the core bottom, whereas the vertical planes give the axial distributions through the middle of the core.

$$i\omega V_f \rho_f(T_{f,0}) c_f(T_{f,0}) \delta T_f(\omega) = -S_{f,surf} h_{m,eff} \left[\delta T_f(\omega) - \delta T_m(\omega)\right] + V_f \delta q'''_f(\omega) \quad (54)$$

In Eq. (54), the effects of the fluctuations of the fuel temperature onto the fuel density and fuel specific heat were neglected. In order to solve the above system of equations, some relationships in terms of fluctuations of the quantities appearing in the equation of state of the fluid needs to be established. In this work, linear approximations are used, thus resulting in the following sets of equations derived from the equation of state:

$$\delta \hat{h}_{k,m}(\omega) = \lambda_{k,m} \delta P_m(\omega) + \beta_{k,m} \delta \rho_{k,m}(\omega) \quad (55)$$

$$\delta \hat{h}^{\pm}_{k,m}(\omega) = \lambda^{\pm}_{k,m} \delta P^{\pm}_m(\omega) + \beta_{k,m} \delta \rho^{\pm}_{k,m}(\omega) \quad (56)$$

and

$$\delta T_m(\omega) = \gamma_m \delta P_m(\omega) + \theta_m \delta \rho_m(\omega) \quad (57)$$

$$\delta T^{\pm}_m(\omega) = \gamma^{\pm}_m \delta P^{\pm}_m(\omega) + \theta^{\pm}_m \delta \rho^{\pm}_m(\omega) \quad (58)$$

where the subscript k in Eqs. (55) and (56) denotes the phase. Eqs. (57) and (58) are only used for single liquid phase situations. The above equations, combined with the dynamic version of Eqs. (37)–(44) allows reformulating the entire thermal–hydraulic dynamic problem into sets of equations where only the fluctuations of the phasic densities, of the mixture velocity, and of equilibrium pressure appear. In case of one-phase flow PWR conditions, the axial variation of the pressure field is negligible. As a result, the linear momentum conservation Eq. (52) is not solved, and the system of equations can be easily solved in each of the flow channels from the inlet of the core to the outlet, with given inlet boundary conditions. In case of two-phase flow BWR conditions, the pressure field needs to be resolved, and the system of equations is solved in an iterative manner as follows. The axial distributions of the pressure and densities are first assumed, the axial variation of the velocity from the inlet to the outlet is then determined, followed by the re-calculation of the axial variation of the density from the inlet to the outlet. Based on the computed distributions, the pressure field is updated from the outlet to the inlet of the fuel channels, and the process is repeated until convergence. Further details about the calculation procedure can be found in Dykin et al. (2014).

The thermal–hydraulic static solver was successfully benchmarked for a number of test cases summarized below:

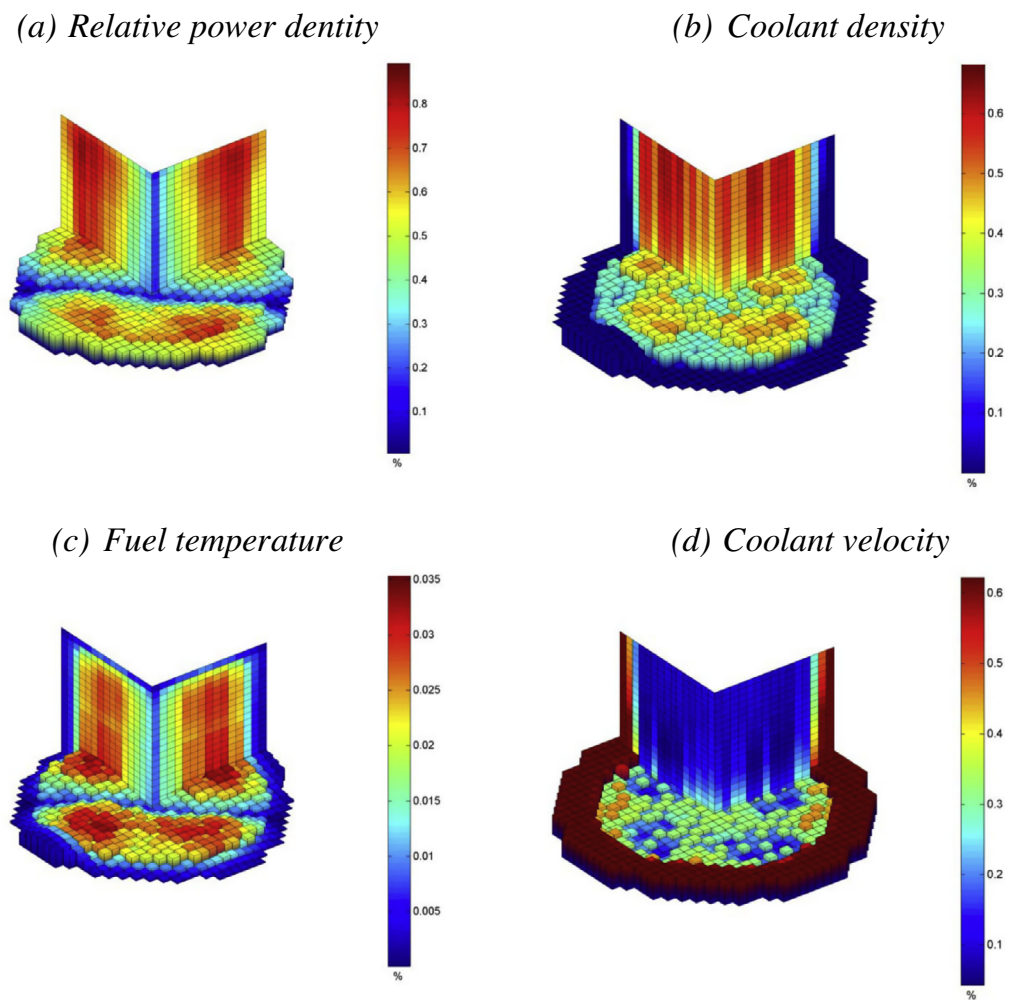

Fig. 6. Three-dimensional distributions of the amplitude of the stationary fluctuations of the neutronic and thermal–hydraulic variables (BWR example). The horizontal planes give the radial distributions at ¼ elevation from the core bottom, whereas the vertical planes give the axial distributions through the middle of the core.

- A heterogeneous three-dimensional PWR core [see Larsson and Demazière (2012)].
- A heterogeneous three-dimensional BWR core [see (Dykin et al. (2014)].

The above two test cases were run using static commercial core simulators, with neutronic feedback included. Likewise, the tool reported in this paper was also used for these verification cases with neutronic feedback included (see Section 2.3 for a description of the coupling procedure for the tool). For the dynamic solver, no other code having the same capabilities exists. Due to the non-analytical form of the equation of state of the fluid, the derivation of analytical solutions is impossible. The code has nevertheless been benchmarked against:

- The CFD code FLUENT for a single assembly thermal–hydraulic test case (without neutronic feedback).
- The RELAP5/PARCS codes for a heterogeneous three-dimensional PWR core (with neutronic feedback).

Some discrepancies between the simulations performed by the present tool and the results of the FLUENT and RELAP5/PARCS simulations were noticed. Nevertheless, when such discrepancies occurred, the FLUENT and RELAP5/PARCS solutions were non-physical, whereas the solution computed by the numerical tool always gave physically-sound results. This further highlights the advantages of the developed tool, as compared to the existing time-domain codes. Further explanations about these test cases and the interpretation of the differences can be found in Larsson and Demazière (2012).

2.3. Coupling methodology

The thermal–hydraulic and neutronic models are coupled via two sets of data for both the static and the dynamic calculations: the dependence of the macroscopic cross-sections on the thermal–hydraulic variables, and the dependence of the power density on the neutronic variables. Concerning the macroscopic cross-sections, a dependence on moderator density and fuel temperature is assumed, i.e.:

$$\Sigma_{\chi,g,n}(t) \approx \varepsilon_{\chi,g,n}[\rho_m(t)] + \eta_{\chi,g,n}[T_f(t)] \tag{59}$$

where the subscripts χ and g represents the reaction type and the energy group, respectively. The tool allows either table-based or polynomial-based dependencies to be used for the functions $\varepsilon_{\chi,g,n}$ and $\eta_{\chi,g,n}$, and the dependence of the macroscopic cross-sections on fuel temperature and moderator density has thus to be defined by the user (no linear dependence needs to be assumed). Concerning the power density, the volumetric power is related to the fission reaction rates as:

$$q'''_f(t) = \kappa[\Sigma_{f,1,n}(t)\phi_{1,n}(t) + \Sigma_{f,2,n}(t)\phi_{2,n}(t)] \tag{60}$$

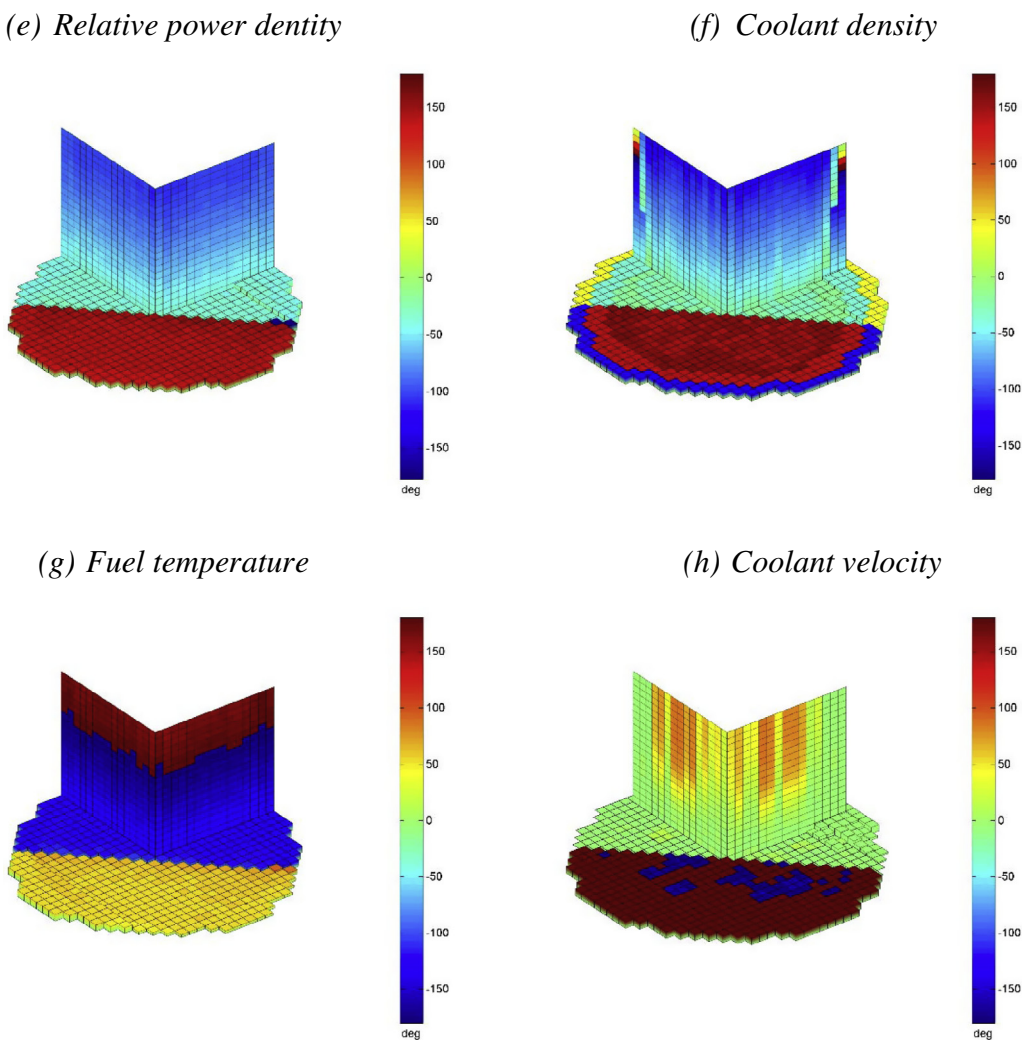

Fig. 7. Three-dimensional distributions of the phase of the stationary fluctuations of the neutronic and thermal–hydraulic variables (BWR example). The horizontal planes give the radial distributions at ¼ elevation from the core bottom, whereas the vertical planes give the axial distributions through the middle of the core.

In the above two expressions, it is implicitly assumed that a neutronic node n is mapped to one single node m for the fluid and one single node f for the fuel, for the thermal–hydraulic to neutronic coupling. Likewise, a fuel node f is mapped to one single neutronic node n for the neutronic to thermal–hydraulic coupling.

Both the static and dynamic calculations are performed in an iterative manner. A spatial distribution of the thermal–hydraulic variables is first assumed. The spatial distribution of the macroscopic cross-sections can thus be determined using Eq. (59), and the neutronic problem can thereafter be solved. Based on the spatial distribution of the calculated neutron flux, the spatial distribution of the power density can be known, the thermal–hydraulic problem can be solved accordingly, and the spatial distribution of the thermal–hydraulic variables can be re-calculated. This process is repeated until convergence.

3. Demonstration of the tool

3.1. Input data preparation

Some data should be provided to the tool in order to perform the static and dynamic calculations. In addition to some geometrical data related to the core and the fuel assemblies, the three-dimensional distributions of the functional dependencies $\varepsilon_{\chi,g,n}$ and $\eta_{\chi,g,n}$ representing the variations of the cross-sections with respect to moderator density and fuel temperature, respectively, should be given, as well as the point-kinetic data of the core (fraction β of delayed neutrons and decay constant λ of the precursors of delayed neutrons). Such data can be most easily obtained from commercial static core simulators. It thus means that the modelling of the considered core with a core simulator is required prior to using the numerical tool presented in this paper. Even if the static solution is thus readily available, it is essential to re-compute the static solution with the tool reported in this paper. This is explained by the fact that the dynamic equations are solved with a discretization scheme not necessarily identical with the discretization scheme in use in the external core simulator. Since the governing dynamic equations have been obtained by first subtracting the static solution, assumed to fulfil the time-independent spatially discretized conservation equations, the same discretization scheme has to be used for both the static and dynamic problems.

In addition, and in order to avoid using too many thermal–hydraulic correlations, the spatial distribution of the effective heat transfer coefficient, as defined in Eq. (35), should also be provided to the tool, using Eq. (36) and the corresponding solution provided by the external core simulator. Finally, a recalibration of the void fraction, when two-phase flow conditions are encountered should be carried out, using the slip ratio also provided by the external core simulator, as earlier explained in Eqs. (43) and (44).

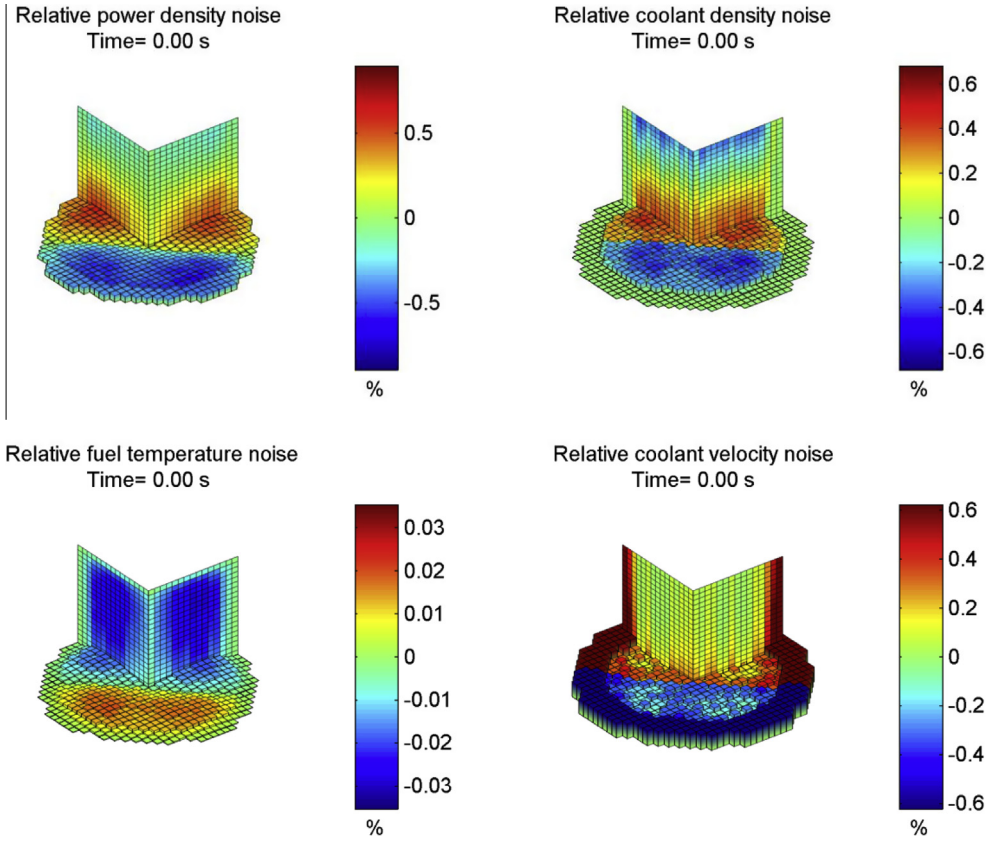

Fig. 8. Snapshot of the time-domain simulations showing the three-dimensional distributions of the stationary fluctuations of the neutronic and thermal–hydraulic variables (BWR example). The horizontal planes give the radial distributions at ¼ elevation from the core bottom, whereas the vertical planes give the axial distributions through the middle of the core.

3.2. PWR example

In the following, a PWR example is considered. The input data were obtained from processing of the results of static core calculations performed with SIMULATE-3 (Covington et al., 1995). Fig. 1 represents the three-dimensional distributions of the static relative power density, coolant density, fuel temperature, and coolant velocity. As can be seen in this figure, the fuel temperature closely follows the relative power density. Because of the one-phase nature of the flow, the variation of the coolant density through the core is mild. Due to mass conservation and decrease of the coolant density from bottom to top, the coolant velocity increases accordingly. Figs. 2 and 3 give the three-dimensional distributions of the amplitude and of the phase, respectively, of the stationary fluctuations at a frequency of 0.5 Hz induced by a perturbation applied on the coolant temperature at the inlet of the core. This perturbation is defined as being homogeneous in amplitude, but out-of-phase between the two halves of the core. Fig. 3 clearly highlights the corresponding radially asymmetrical response of the neutron flux and of the fuel temperature. From the amplitude and phase of the computed variables, an inverse Fourier transform can be performed, in order to estimate the time-dependence of the different variables throughout the core. A snapshot of a time-domain simulation can be found in Fig. 4, where the phase shift between different spatial points and between the different variables can be seen. By noticing the axial variation of the perturbations in coolant density, the transport of the applied perturbation from the inlet to the outlet of the core can be seen. The animation also distinctly highlights such an axial transport of the inlet perturbations with the flow.

3.3. BWR example

In the following, a BWR example is considered. The input data were obtained from processing of the results of static core calculations performed with POLCA-7 (Lindahl, 2007). Fig. 5 represents the three-dimensional distributions of the static relative power density, coolant density, fuel temperature, and coolant velocity. Contrary to the PWR example, the variation of the coolant density between the core inlet and outlet is very significant, because of vapour production. Correspondingly, the flow accelerates drastically. Figs. 6 and 7 give the three-dimensional distributions of the amplitude and of the phase, respectively, of the stationary fluctuations at a frequency of 0.5 Hz induced by a perturbation applied on the coolant velocity at the inlet of the core. This perturbation is defined as being homogeneous in amplitude, but out-of-phase between the two halves of the core. As for the PWR case for a perturbation in the inlet coolant density, the responses of the neutron flux and correspondingly of the fuel temperature are radially asymmetrical. From the amplitude and phase of the computed variables, an inverse Fourier transform can be performed, in order to estimate the time-dependence of the different variables throughout the core. A snapshot of a time-domain simulation can be found in Fig. 8, where the phase shift between different spatial points and between the different variables can be seen. As for the PWR case, the axial transport of the inlet perturbations upwards with the flow is clearly visible. This can be seen by examining the axial variation of the perturbations in coolant density. In addition, one also notices that the amplitude of the fluctuations in coolant density and velocity is much larger than in the PWR case, because of the two-phase nature of the flow.

4. Discussion and conclusions

The development of a three-dimensional simulator able to model stationary fluctuations in nuclear cores was reported in this paper. This simulator, currently available in Matlab, handles both PWR and BWR conditions, and tackles the modelling of neutron transport, fluid dynamics, heat transfer, and their corresponding coupling mechanisms. The modelling of neutron transport relies on the two-group diffusion approximation, whereas the spatial discretization is based on finite differences. For the modelling of heat transfer, the heat conduction equation is solved in the fuel pins in the radial direction, with the use of an effective heat transfer coefficient. For the modelling of fluid dynamics, the HEM is used, with a correction of the void fraction using the slip ratio. The spatial discretization of the HEM and of the heat transfer model is based on finite volumes. Both the effective heat transfer coefficient and the slip ratio are computed by an external core simulator, used to provide the necessary data to the numerical tool. Such data also include the nodal macroscopic cross-section dependence on fuel temperature and moderator density, as well as the point-kinetic parameter of the core. Providing the above data from another core simulator allows limiting the use of correlations in the numerical tool developed, thus making it very versatile and generic.

The developed tool, verified in a number of test cases, is the only of its kind, and allows modelling the transport of fluctuations in nuclear cores in the frequency domain with a high level of reliability. The modelling of stationary fluctuations using existing and well established time-domain simulation platforms has been demonstrated to suffer from numerical diffusion, and the results obtained are in some cases non-physical (Larsson and Demazière, 2012).

The neutronic part of the tool has already been successfully used in many applications [see e.g. (Demazière and Pázsit, 2009) and (Demazière, 2011a)]. More recently, the coupled version of the tool was used in a PWR set-up to study the possibility to determine using noise analysis the Moderator Temperature Coefficient (MTC) of reactivity (Demazière and Larsson, 2012) in PWRs. The novelty of this investigation also resides in the fact that the calculations were carried out using a measured spectrum for the inlet temperature fluctuations. The calculations were thus performed at several frequencies, and the spectrum of the resulting induced fluctuations was reconstructed.

After the successful development and verification of the tool, work is planned to be devoted to improve the accuracy of the simulations by using more sophisticated models. Some parts of the tool have already been extended. For instance, the development of a multi-group diffusion based solver able to handle hexagonal fuel assembly types has been carried out (Tran et al., 2013), with the tool thus being able to handle among other things fast systems. The tool could also be extended to investigate the effect of structural disturbances, by including in the system of equations possible stationary fluctuations of the geometrical parameters of the system.

Acknowledgements

The authors wish to express their appreciation to Dr. Carl Sunde and MSc. Filippo Zinzani, who contributed, either via discussions or active participation, to the development of the tool. Prof. Imre Pázsit is also acknowledged for his long-term support during this project.

The continued financial support from the Swedish nuclear industry via different projects, for which the development of the tool was necessary, is also deeply acknowledged, and among others Ringhals AB (Research contracts: 522351-003, 531970-003, 543672-002, 557700-003, 566379-003, and 578254-003), the Swedish Radiation Safety Authority SSM (formerly the Swedish Nuclear Power Inspectorate SKI – Research Contracts: 14.5-991060-99180, 14.5-000983-00156, 14.5-010892-01161, 14.5-011142-01261, SSM2012-3299, and SSM2013-903), and the Nordic Thermal–Hydraulic Network NORTHNET [Research Contracts: 4500131026 (Forsmark Kraftgrupp AB), 581422-025 (Ringhals AB), SKI 2007/1588/200705015 (Swedish Radiation Safety Authority SSM – formerly the Swedish Nuclear Power Inspectorate), and SE 08-018g (Westinghouse Electric Sweden AB)].

Appendix A. Supplementary data

Supplementary data associated with this article can be found, in the online version, at http://dx.doi.org/10.1016/j.anucene.2014.09.042.

References

Chisholm, D., 1973. Pressure gradients due to friction during the flow of evaporating two-phase mixtures in smooth tubes and channels. Int. J. Heat Mass Transf. 16, 347–358.

Covington, L.J., Cronin, J.T., Umbarger, J.A., 1995. SIMULATE-3: advanced three-dimensional two-group reactor analysis code. Studsvik Scandpower, report Studsvik/SOA-95/15 Rev 2.

Davis, T.A., 2002. UMFPACK Version 4.6 User Guide. Department of Computer and Information Science and Engineering, University of Florida, Gainesville, FL, USA.

Demazière, C., 2011a. CORE SIM: a multi-purpose neutronic tool for research and education. Ann. Nucl. Energy 38, 2698–2718.

Demazière, C., 2011b. Description of the models and algorithms used in the CORE SIM neutronic tool. Report CTH-NT-241, Chalmers University of Technology, Gothenburg, Sweden.

Demazière, C., 2011c. Validation and demonstration of the CORE SIM neutronic tool. Report CTH-NT-242, Chalmers University of Technology, Gothenburg, Sweden.

Demazière, C., Larsson, V., 2012. Investigation of the MTC noise estimation with a coupled neutronic/thermal-hydraulic dedicated model – "Closing the loop". In: Proceedings of the International Conference on Advances in Reactor Physics – Linking Research, Industry, and Education (PHYSOR 2012), Knoxville, TN, USA, April 15–20, 2012, American Nuclear Society.

Demazière, C., Pázsit, I., 2009. Numerical tools applied to power reactor noise analysis. Prog. Nucl. Energy 51, 67–81.

Dokhane, A., 2004. BWR Stability and Bifurcation Analysis using a Novel Reduced Order Model and the System Code RAMONA (Ph.D. dissertation), EPFL, Switzerland.

Dykin, V., Hernández-Solís, A., Demazière, C., 2014. Further development of the core simulator CORE SIM: Extension to coupled capabilities for BWRs. Report 2014:09, Strålsäkerhetsmyndingheten (SSM – the Swedish Radiation Safety Authority), Stockholm, Sweden.

Larsson, V., Demazière, C., 2009. Comparative study of 2-group P1 and diffusion theories for the calculation of the neutron noise in 1D 2-region systems. Ann. Nucl. Energy 36, 1574–1587.

Larsson, V., Demazière, C., 2012. A coupled neutronics/thermal–hydraulics tool for calculating fluctuations in Pressurized Water Reactors. Ann. Nucl. Energy 43, 68–76.

Lindahl, S.-Ö., 2007. POLCA7-BWR core simulator. Westinghouse Atom AB, report BR 94–700, Rev. 2.

Rust, J.H., 1979. Nuclear Power Plant Engineering. Haralson Publishing Company, Atlanta, USA.

Shah, R.K., Sekulic, D.P., 2003. Fundamentals of Heat Exchanger Design. John Wiley & Sons, Inc..

Tran, H.N., Zylbersztejn, F., Demazière, C., Jammes, C., Filliatre, P., 2013. A multi-group neutron noise simulator for fast reactors. Ann. Nucl. Energy 62, 158–169.